Excitation-contraction coupling alterations in mdx and utrophin/dystrophin double knockout mice: a comparative study

Joana Capote, Marino DiFranco and Julio L. Vergara

Am J Physiol Cell Physiol 298:1077-1086, 2010. First published Feb 3, 2010;
doi:10.1152/ajpcell.00428.2009

Am J Physiol Cell Physiol 298: C1077–C1086, 2010.
First published February 3, 2010; doi:10.1152/ajpcell.00428.2009.

Excitation-contraction coupling alterations in *mdx* and utrophin/dystrophin double knockout mice: a comparative study

Joana Capote, Marino DiFranco, and Julio L. Vergara

Department of Physiology, David Geffen School of Medicine, University of California, Los Angeles, California

Submitted 22 September 2009; accepted in final form 1 February 2010

Capote J, DiFranco M, Vergara JL. Excitation-contraction coupling alterations in *mdx* and utrophin/dystrophin double knockout mice: a comparative study. *Am J Physiol Cell Physiol* 298: C1077–C1086, 2010. First published February 3, 2010; doi:10.1152/ajpcell.00428.2009.—The double knockout mouse for utrophin and dystrophin ($utr^{-/-}$/*mdx*) has been proposed to be a better model of Duchenne Muscular Dystrophy (DMD) than the *mdx* mouse because the former displays more similar muscle pathology to that of the DMD patients. In this paper the properties of action potentials (APs) and Ca^{2+} transients elicited by single and repetitive stimulation were studied to understand the excitation-contraction (EC) coupling alterations observed in muscle fibers from *mdx* and $utr^{-/-}$/*mdx* mice. Based on the comparison of the AP durations with those of fibers from wild-type (WT) mice, fibers from both *mdx* and $utr^{-/-}$/*mdx* mice could be divided in two groups: fibers with WT-like APs (*group 1*) and fibers with significantly longer APs (*group 2*). Although the proportion of fibers in *group 2* was larger in $utr^{-/-}$/*mdx* (36%) than in *mdx* mice (27%), the Ca^{2+} release elicited by single stimulation was found to be similarly depressed (32–38%) in $utr^{-/-}$/*mdx* and *mdx* fibers compared with WT counterparts regardless of the fiber's group. Stimulation at 100 Hz revealed that, with the exception of those from $utr^{-/-}$/*mdx* mice, *group 1* fibers were able to sustain Ca^{2+} release for longer than *group 2* fibers, which displayed an abrupt limitation even at the onset of the train. The differences in behavior between fibers in *groups 1* and *2* became almost unnoticeable at 50 Hz stimulation. In general, fibers from $utr^{-/-}$/*mdx* mice seem to display more persistent alterations in the EC coupling than those observed in the *mdx* model.

muscular dystrophy; mammalian skeletal muscle; fluorescence microscopy

DMD, the most common and severe form of childhood muscular dystrophy, results from mutations in the dystrophin gene that lead to lack or nonfunctional expression of the membrane-associated cytoskeletal protein dystrophin (10, 18, 20, 25). In healthy muscle, dystrophin is proposed to act as a linker between the cytoskeleton and the extracellular matrix through its interaction with proteins of the dystrophin-glycoprotein complex (DGC) located on the plasma membrane (17). Most of the current knowledge about DMD pathophysiology comes from studies using the *mdx* mouse as a model because it lacks the expression of dystrophin. Furthermore, in both *mdx* mice and DMD patients, muscles undergo multiple muscle fiber degeneration/regeneration cycles and display reduced specific active force (18, 28). In this regard, it is noteworthy that the reduction in the Ca^{2+} release from the sarcoplasmic reticulum (SR) evoked by single AP stimulation (16, 30) in fibers from flexor digitorum brevis (FDB) muscles of *mdx* mice (with respect to WT mice) may explain the muscle weakness. Our laboratory further demonstrated that the voltage dependence of the excitation-contraction (EC) coupling process is not altered in *mdx* muscle fibers, and that the Ca^{2+} release limitation was not related to obvious changes in the properties of the APs nor to noticeable alterations in the structure or electrical characteristics of the transverse tubular system (TTS) (9, 29, 30).

Despite its attractiveness as a model for DMD, *mdx* mice, unlike DMD patients, have a nearly normal lifespan and do not develop severe myofibrosis and cardiomyopathy (5, 6, 13). As an explanation for the relatively mild pathophysiology exhibited by *mdx* mice, it has been suggested that utrophin, a dystrophin homologue coded by an autosomic gene (13, 25) and overexpressed in *mdx* mice, can compensate for the lack of dystrophin. In support of this hypothesis, two different groups (6, 13) developed a double knockout mouse for utrophin and dystrophin ($utr^{-/-}$/*mdx*) and discovered that these mice are smaller than age-matched WT mice and display pronounced kyphosis, progressive muscle wasting, impaired mobility, and premature death. Altogether, research with this animal model has revealed that, though not an authentic genetic model of DMD, the $utr^{-/-}$/*mdx* mouse better recapitulates the overall human pathology than the *mdx* mouse.

The purpose of the current work was to investigate whether the more severe phenotype of $utr^{-/-}$/*mdx* mice is associated with a worsening of the impairment in the EC coupling seen in *mdx* muscle fibers. Overall, we found that fibers from $utr^{-/-}$/*mdx* mice display a similar impairment in the Ca^{2+} release to that observed in *mdx* muscle fibers. However, these limitations become complicated by alterations in the electrical properties of the fibers, which are particularly pervasive in a subpopulation of fibers from the $utr^{-/-}$/*mdx* animal model. We further demonstrate that high-frequency stimulation (e.g., 100 Hz), which is more akin the normal pattern of stimulation of mammalian skeletal muscle fibers under central nervous system (CNS) control (14), help to unmask intrinsic limitations in the EC coupling process, which may not be readily observable with low frequency or single pulse stimulation. A preliminary version of this work has been presented to the Biophysical Society (4).

MATERIALS AND METHODS

All the procedures involving animals were approved and carried out according to the guidelines of the UCLA Animal Care Committee. WT mice (C57Bl/10J) were purchased from the Jackson Laboratories (Bar Harbor, ME), and *mdx* (C57BL/10ScSn-mdx/J) and $utr^{-/-}$/*mdx* mice (>2–3 mo old) came from colonies established in our laboratory using founders obtained from the Jackson Laboratories and from Dr. J. R. Sanes, respectively. Genotyping was done by using PCR protocols as previously described (1, 12). Isolated fibers from FDB or interosseus (IO) muscles were obtained by enzymatic dissociation [40 min treatment with 3 mg/ml collagenase type 2 (Worthington) in a shaking bath (40 spm at 36°C) (29)]. Since FDB and IO muscles from

Address for reprint requests and other correspondence: J. L. Vergara, Dept. of Physiology, David Geffen School of Medicine, UCLA, 10833 Le Conte Ave., Los Angeles, CA 90095-1751 (e-mail: jvergara@mednet.ucla.edu).

Table 1. *Dimensions of muscle fibers isolated from WT, mdx, and utr$^{-/-}$/mdx mice*

Mice Strain	*n*	Fiber Diameter, μm	Fiber Length, μm
WT	27	42.6 ± 9.9	456 ± 7
mdx	28	41.5 ± 7.9	479 ± 8
utr$^{-/-}$/mdx	22	36.2 ± 8.6*	409 ± 8*

Values are means ± SD; *n* is the number of mice. WT, wild-type mice; *mdx*, dystrophin mice; *utr*, utrophin mice. *utr$^{-/-}$/mdx,* double knockout mice for utrophin and dystrophin. *$P < 0.05$ ANOVA unpaired *t*-test comparison with WT values.

utr$^{-/-}$/mdx mice contain fibers of smaller diameter than those from *mdx* and WT mice (see Table 1), all the experiments were performed in small fibers while attempting to match their diameters. In addition, only nonbranched muscle fibers were used.

Electrophysiological techniques. A two-microelectrode amplifier was used to stimulate the fibers and to record the membrane potential as described previously (9, 29, 30). Both current and voltage electrodes were filled with an internal solution containing (in mM): 78 K-aspartate, 30 EGTA, 15 $Ca(OH)_2$, 20 K-MOPS, 5 ATP disodium, 5 $MgCl_2$, 5 phosphocreatine disodium, and 5 glutathione, plus 0.1 g/l phosphocreatine kinase; pH adjusted to 7.2 with KOH. The resistance of the electrodes was ~10 MΩ. The composition of the external Tyrode solution was (in mM): 145 NaCl, 5 KCl, 2 $CaCl_2$, 1 $MgCl_2$, 10 Na-MOPS, and 10 dextrose; pH 7.2. The resting potential of the fibers was maintained at −90 mV by the injection of a small steady current through the current electrode (<15 nA, see Ref. 30); fibers requiring more than 15 nA were discarded. Single suprathreshold current pulses of 0.5 ms in duration, or trains of 30 pulses of the same duration delivered at frequencies ranging from 25 to 100 Hz, were used. The pulse amplitude was in the range of 200–300 nA. A resting period of 2 min was allowed between consecutive single pulse stimulations or 5 min between trains.

Ca^{2+} release measurements. Intracellular Ca^{2+} concentration changes elicited by single APs, or trains of APs, were detected by using the low-affinity fluorescent Ca^{2+} indicator Oregon Green BAPTA-5N [OGB-5N (Invitrogen), 250 μM]. Fluorescence changes, hereafter called OGB-5N transients, or Ca^{2+} transients, are normalized in ΔF/F units (8, 29, 30). A period of 30 min was allowed for dye diffusion and equilibration before starting the stimulation protocols. The optical setup used for global illumination/detection is based on an inverted fluorescence microscope (IX-70, Olympus, Japan). A 100-W tungsten-halogen lamp was used as a source of light, and excitation/emission wavelengths were selected using the following filter combination: 460–500 nm/505DRLP/512-558 nm (excitation/dichroic/emission; Chroma). A photodiode (UV-100, UDT) connected to a patch-clamp amplifier (Axopatch 200A, Axon Instruments) was used to detect the OGB-5N fluorescence. Experiments were performed at room temperature (18–19°C).

Data acquisition, analysis, and statistics. Electrical and optical data were acquired simultaneously, filtered at 5 kHz, and digitized with 16-bits resolution. The amplitude of APs and OGB-5N transients was calculated as the difference between peak and prestimulus (or interpulse) values as shown in Fig. 1. The ratio A_2/A_1, where A_2 and A_1 correspond to the amplitudes of the second and first OGB-5N transients of a train, respectively (Fig. 1), was calculated to measure the abrupt depression in Ca^{2+} release occurring in this particular interval. The full duration at half-maximum (FDHM) of the signals (APs and OGB-5N transients) were measured as described previously (30).

For single pulse stimulation, Ca^{2+} release fluxes were calculated from theoretical predictions with parameters adjusted to fit experimental ΔF/F transients using a single compartment model as previously described (9, 29, 30). Here, we used the following kinetic parameters for the OGB-5N dye: $k_{on} = 0.16\ \mu M^{-1}\cdot ms^{-1}$, $k_{off} = 8\ ms^{-1}$, and $F_{max}/F_{min} = 37$. They provided the best prediction (data not shown) of equilibrium and kinetic dye calibrations using DM-nitrophen flash photolysis techniques (11, 19). The concentrations and properties of the main endogenous buffers were reported previously (9, 29, 30) and assumed the same for all the fiber types in this work. For repetitive stimulation, the theoretical model was modified to allow for the generation of multiple Ca^{2+} transients; the decay of the amplitudes of the modeled Ca^{2+} transients during the train was adjusted using a double-exponential function to predict the experimental data.

Unless otherwise indicated, the experimental results were expressed as means ± SD of *n* observations. Sets of data were compared using Student's *t*-test with $P < 0.05$.

RESULTS

Morphological characteristics of utr$^{-/-}$/mdx skeletal muscle fibers. FDB and IO muscles in *utr$^{-/-}$/mdx* mice are smaller than those in age-matched *mdx* and WT mice. Despite this morphological difference, enzymatic dissociation of *utr$^{-/-}$/mdx* muscles yields a large amount of healthy fibers. This suggests that *utr$^{-/-}$/mdx* muscle fibers actually do not display greater fragility compared with WT and *mdx* counterparts. As shown in Table 1, the diameter of dissociated fibers from *utr$^{-/-}$/mdx* FDB and IO muscles is variable; nevertheless, the fibers are shorter and thinner than those from WT and *mdx* muscles. Branched fibers are less abundant in *utr$^{-/-}$/mdx* than in *mdx* muscle fibers but, when present, the branches were considerably smaller in diameter than those in *mdx* fibers (data not shown). Because of the morphological differences among fibers from the three strains, we decided to use only nonbranched fibers with similar dimensions.

Action potentials and Ca^{2+} signals in utr$^{-/-}$/mdx fibers. Since a goal of this work is to investigate whether knocking off the expression of utrophin in an *mdx* background resulted in further impairment of the EC coupling beyond what has been found in fibers from *mdx* mice (9, 16, 29, 30), APs and OGB-5N fluorescence transients were simultaneously recorded from WT, *mdx*, and *utr$^{-/-}$/mdx* fibers (Fig. 2). It is apparent from Fig. 2*A* that while the durations of the APs recorded from WT (solid trace) and *mdx* fibers (dashed trace) are almost identical, the one from the *utr$^{-/-}$/mdx* fiber (dotted trace) is longer. Figure 2*B* shows that though the OGB-5N transient recorded from the *utr$^{-/-}$/mdx* muscle fiber is ~32% smaller than that from a WT fiber, it is not significantly different from

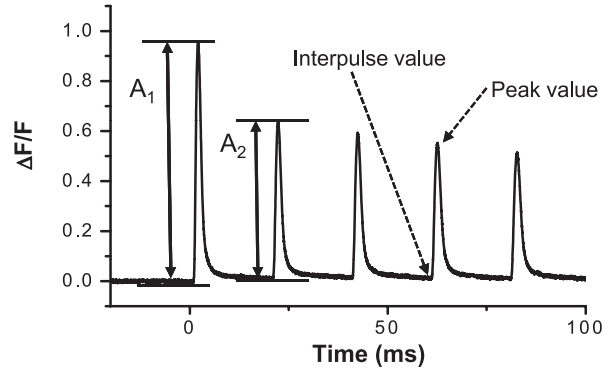

Fig. 1. Signal parameters. Example of OGB-5N transients recorded in response to 50 Hz stimulation. Critical parameters that will be used to characterize both the electrical and the optical signals obtained in response to a train of pulses are shown. Throughout the text, the amplitude of the signals will be calculated as: (peak value − interpulse value).

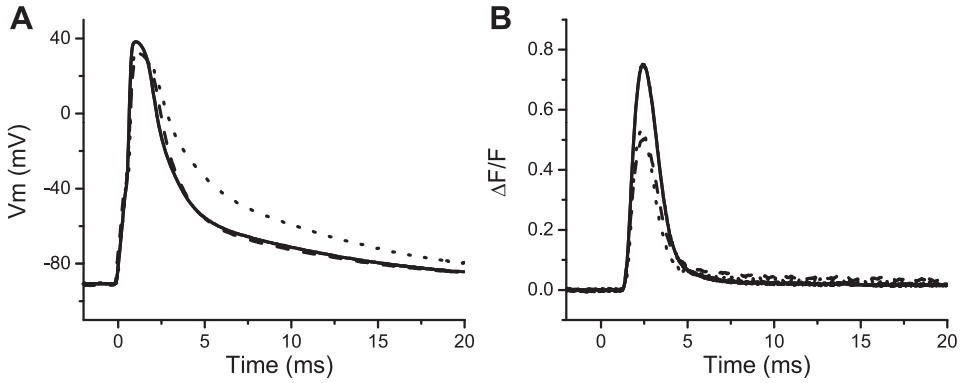

Fig. 2. Action potential (APs) and Oregon Green BAPTA-5N (OGB-5N) transients recorded from WT, *mdx*, and *utr*$^{-/-}$*/mdx* fibers. *A*: superimposed APs recorded from WT (solid trace), *mdx* (dashed trace), and *utr*$^{-/-}$*/mdx* (dotted trace) fibers in response to a single pulse of stimulation. AP peak (mV) and full duration at half-maximum (FDHM, in ms) were 128 and 2.46; 123 and 2.73; and 123 and 3.9 for the WT, *mdx*, and *utr*$^{-/-}$*/mdx* fiber, respectively. *B*: typical OGB-5N transients elicited by single AP in WT (solid trace), *mdx* (dashed trace), and *utr*$^{-/-}$*/mdx* (dotted trace) fibers. ΔF/F peak and FDHM (in ms) of OGB-5N transients were 0.75 and 1.68; 0.50 and 1.8; and 0.52 and 1.5; for the WT, *mdx*, and *utr*$^{-/-}$*/mdx* fiber, respectively.

that recorded from the *mdx* fiber (~38% smaller than WT), despite the aggravated phenotype and/or the prolongation of the AP exhibited by the *utr*$^{-/-}$*/mdx* fibers.

Mean values of the amplitudes and durations of APs and OGB-5N transients of pooled data recorded from WT, *mdx*, and *utr*$^{-/-}$*/mdx* fibers are shown in Table 2. The most relevant result regarding the electrical activity in the three populations of fibers is that both the amplitudes and durations of the APs recorded from *utr*$^{-/-}$*/mdx* muscle are significantly altered with respect to those of WT and *mdx* fibers. Namely, Table 2 shows that the AP amplitude is reduced by ~6.5%, and the FDHM is increased by ~46% in *utr*$^{-/-}$*/mdx* fibers with respect to their WT counterparts, whereas *mdx* fibers did not display significant differences. It can also be observed from Table 2 that fibers from *mdx* and *utr*$^{-/-}$*/mdx* mice display a significant reduction in the amplitude of the OGB-5N transients (~38 and 32%, respectively) when compared with the WT ones ($P < 0.001$). In contrast, differences in the amplitudes of OGB-5N transients between *mdx* and *utr*$^{-/-}$*/mdx* fibers are not significant ($P > 0.3$). Though individual OGB-5N transients in Fig. 2*B* seem to display similar durations, data in Table 2 reveal a slight prolongation in the FDHM of OGB-5N transients recorded from *mdx* fibers with respect to those from WT fibers (from ~1.6 to 1.8 ms, $P < 0.02$); a comparable prolongation was not significant for transients from *utr*$^{-/-}$*/mdx* fibers ($P > 0.07$). In agreement with previous reports, the peak Ca^{2+} release flux calculated from OGB-5N transients of *mdx* fibers (150.3 ± 32.1 μM/ms) was significantly smaller than that of their WT counterparts (242.4 ± 58.4 μM/ms). *Utr*$^{-/-}$*/mdx* fibers also showed a depressed Ca^{2+} release flux, calculated to be 165.7 ± 47.3 μM/ms, which is ~32% smaller than that in WT fibers.

A detailed statistical analysis of the distribution of amplitudes and durations of the APs in fibers from the three mice strains was performed to uncover possible sources of variability in the data contained in Table 2. Figure 3 shows frequency histograms of the amplitudes (Fig. 3, *A*, *C*, and *E*) and durations (Fig. 3, *B*, *D*, and *F*) of the APs recorded from WT (open bars), *mdx* (hatched bars), and *utr*$^{-/-}$*/mdx* (double-hatched bars) fibers. The histogram in Fig. 3*A* shows that the AP amplitudes recorded from WT fibers fall within a normal distribution curve centered at 124.8 mV with a width of 14.2 mV (2×SD). This curve is also shown superimposed with the corresponding data from *mdx* (Fig. 3*C*) and *utr*$^{-/-}$*/mdx* (Fig. 3*E*). It can be seen that most of the AP amplitudes measured from *mdx* fibers are enclosed within the same normal distribution of the WT mice, demonstrating that the amplitudes of APs in these two populations of fibers are not significantly different from each other. AP amplitudes in *utr*$^{-/-}$*/mdx* mice, on the other hand, are weighed toward smaller values; ~73% of *utr*$^{-/-}$*/mdx* fibers display AP amplitudes that fall within the normal distribution of AP amplitudes from WT fibers, but the remaining ~27% of the fibers have AP amplitudes smaller than those from WT fibers (Table 3).

As shown in Fig. 3*B*, the distribution of the FDHM of APs from WT fibers is described by a Gaussian distribution centered at 2.17 ms with a width of 0.96 ms. Those from *mdx* fibers (Fig. 3*D*), though more widely distributed and shifted toward slightly longer values, are still within the range of the normal distribution from WT fibers. In contrast, ~36% of the APs recorded from *utr*$^{-/-}$*/mdx* fibers exhibit FDHM values that are significantly longer than those from WT fibers (Fig. 3*F* and see Table 3).

The distributions of AP amplitudes and FDHMs shown in Fig. 3 suggests that fibers from *mdx* and *utr*$^{-/-}$*/mdx* muscles constitute functionally heterogeneous populations, when compared with those from WT muscles. To further investigate the EC coupling properties of these populations of fibers, we defined two groups using the FDHM of their APs as a criterion: *group 1* (for both *mdx* and *utr*$^{-/-}$*/mdx* mice) included fibers with APs FDHMs within 95% (average ± 2×SD) of those in WT fibers, and *group 2* included fibers displaying values

Table 2. *Amplitude and duration of APs and OGB-5N transients from control, mdx, and utr*$^{-/-}$*/mdx fibers*

		AP		ΔF/F		
Mice Strain	*n*	Amplitude, mV	FDHM, ms	Amplitude	FDHM, ms	Peak Ca^{2+} Release Flux, μM/ms
WT	15	124.8 ± 7.1	2.17 ± 0.48	0.79 ± 0.19	1.57 ± 0.18	242.4 ± 58.4
mdx	11	122.6 ± 9.7	2.48 ± 0.68	0.49 ± 0.10*	1.80 ± 0.30*	150.3 ± 32.1*
utr$^{-/-}$*/mdx*	14	116.7 ± 9.5*	3.15 ± 1.25*	0.54 ± 0.15*	1.74 ± 0.29	165.7 ± 47.3*

Values are means ± SD; *n* is the number of mice. APs, action potentials; FDHM, full duration at half-maximum amplitude; OGB-5N, Oregon Green 488 BAPTA-5N.[1] *$P < 0.05$ ANOVA unpaired *t*-test comparison with WT values.

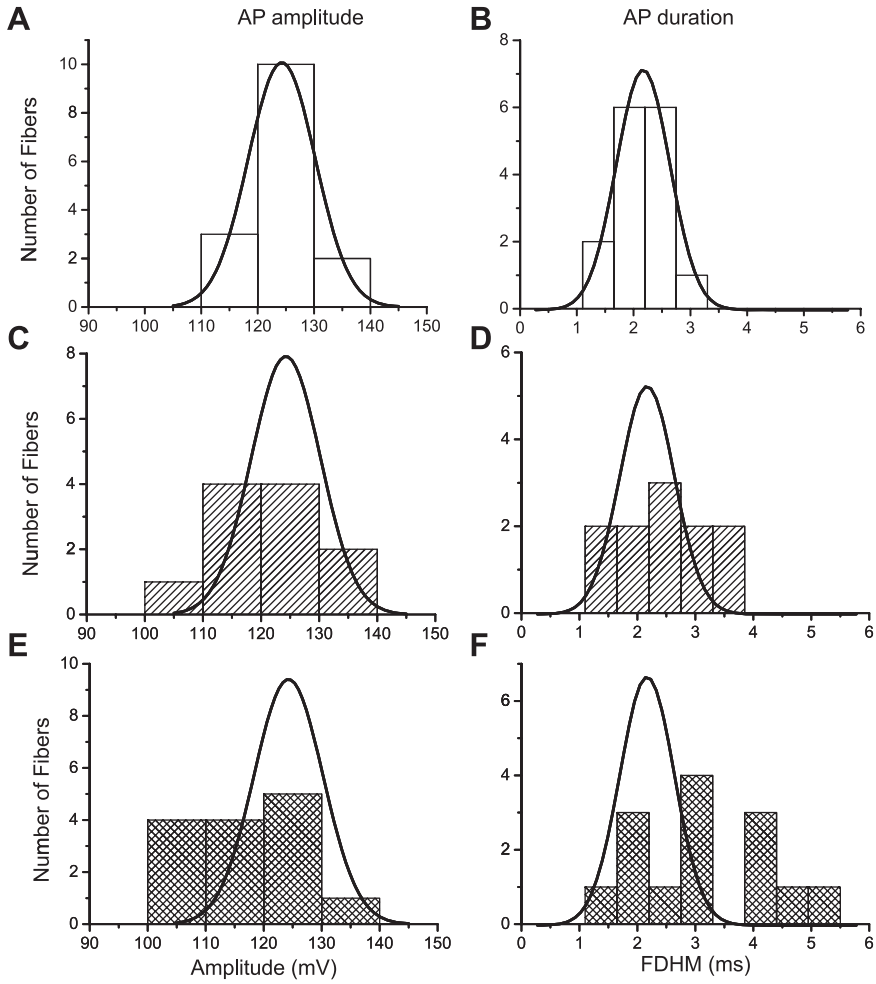

Fig. 3. Frequency histograms of the amplitude and duration of APs recorded from the three mice strains. Histograms of the amplitude and duration of APs recorded (in response to a single pulse) from WT (*A* and *B*), *mdx* (*C* and *D*), and *utr*$^{-/-}$*/mdx* fibers (*E* and *F*). The same binning was used for each parameter. The normal distribution curves for the amplitude and duration data from WT mice (solid lines) are shown superimposed on top of the *mdx* and *utr*$^{-/-}$*/mdx* histograms; they were scaled according to the total number of fibers in each population.

significantly longer. As shown in Table 3, 73% of the fibers from *mdx* mice belong to *group 1* (*mdx*-1), whereas only ~64% of fibers from *utr*$^{-/-}$*/mdx* mice belong to this group (*utr*$^{-/-}$*/mdx*-1). The APs recorded from *mdx*-1 fibers (Fig. 4*B*) and *utr*$^{-/-}$*/mdx*-1 (Fig. 4*C*) are not significantly different in amplitude and duration from those recorded from WT fibers (Fig. 4*A*); in contrast, APs from *mdx*-2 (Fig. 4*D*) and *utr*$^{-/-}$*/mdx*-2 (Figs. 4*E*) fibers are smaller and considerably longer than those from control fibers (see also Table 3). Notably, Fig. 4 and Table 3 show that the amplitude of OGB-5N transients from *mdx* and *utr*$^{-/-}$*/mdx* fibers are similarly impaired with respect to those from WT fibers (29–40% reduction in amplitude) regardless of the disparity in the AP parameters for each group of fibers. However, the FDHM of OGB-5N transients in *mdx*-2 and *utr*$^{-/-}$*/mdx*-2 fibers are significantly longer than those from WT and *group 1* fibers.

APs and Ca^{2+} *transients elicited by high-frequency stimulation in mdx and utr*$^{-/-}$*/mdx fibers.* The CNS controls mechanical output during voluntary movement by recruiting various numbers of motor units and/or by activating the muscle fibers with multiple patterns of stimulation, which in mammals can reach frequencies exceeding 100 Hz (14). Thus it seemed relevant to investigate how is the Ca^{2+} release impairment manifested in both *utr*$^{-/-}$*/mdx* and *mdx* fibers when they are stimulated with patterns that emulate the in vivo situation. We first studied the electrical activity and Ca^{2+} release in response to trains of 30 pulses applied at 100 Hz; as can be seen (Fig. 5*A*), APs with almost constant peak values (approximately +35

Table 3. *AP and OGB-5N transient characterization from groups 1 and 2 of mdx and utr*$^{-/-}$*/mdx fibers*

Fiber Type	*n*	AP		ΔF/F		Peak Ca^{2+} Release Flux, μM/ms
		Peak Value, mV	FDHM, ms	Peak Value	FDHM, ms	
WT	15	124.80 ± 7.06	2.17 ± 0.48	0.79 ± 0.19	1.57 ± 0.18	242.4 ± 58.4
mdx-1	8/11	124.56 ± 10.13	2.18 ± 0.54	0.50 ± 0.12*	1.71 ± 0.29	152.2 ± 36.7*
mdx-2	3/11	117.36 ± 7.41	3.26 ± 0.15*	0.48 ± 0.06*	2.04 ± 0.19*	145.2 ± 19.6*
utr$^{-/-}$*/mdx-1*	9/14	119.90 ± 9.03	2.35 ± 0.61	0.56 ± 0.17*	1.65 ± 0.29	183.8 ± 50.0*
utr$^{-/-}$*/mdx-2*	5/14	111.01 ± 7.96*	4.58 ± 0.61*	0.50 ± 0.12*	1.97 ± 0.14*	144.6 ± 37.2*

Values are means ± SD; *n* is number of mice. *$P < 0.05$ ANOVA unpaired *t*-test comparison with WT values.

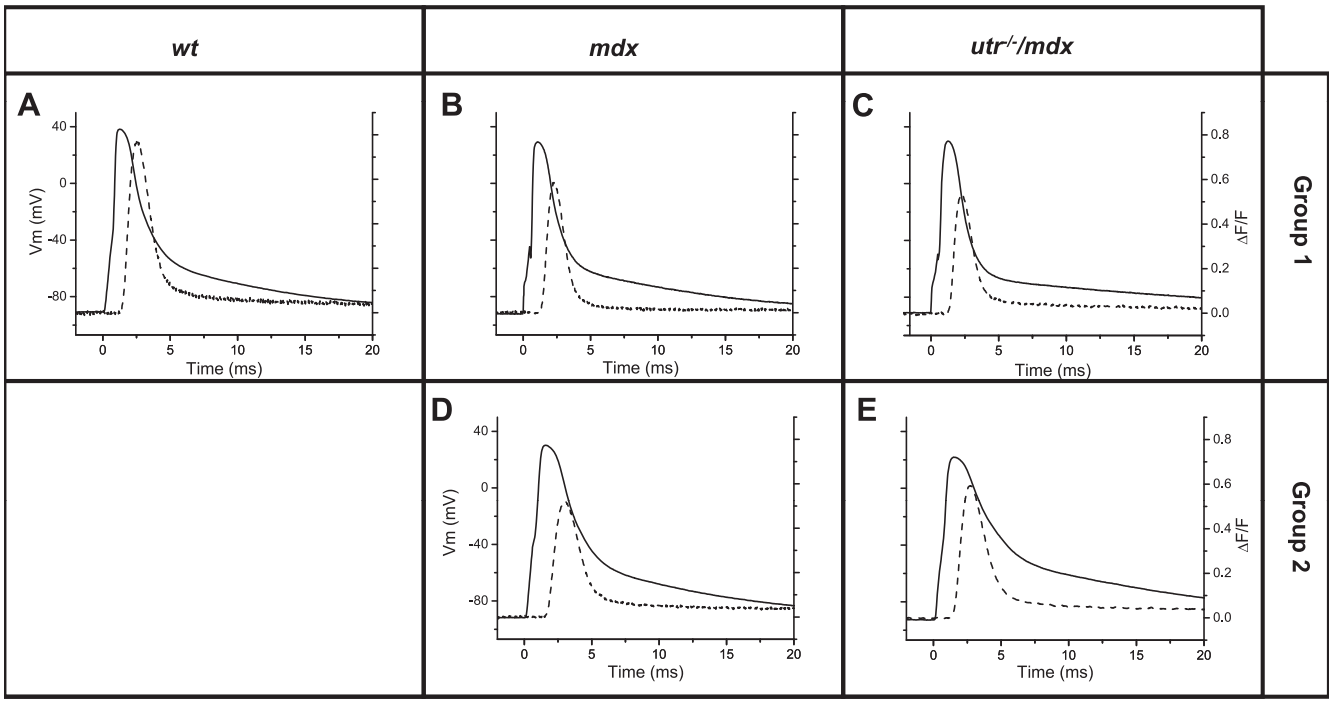

Fig. 4. APs and OGB-5N transients recorded from WT and pregrouped *mdx* and *utr*$^{-/-}$*/mdx* fibers. *A–E*: superimposed electric (solid lines) and OGB-5N (dashed lines) signals responses in response to single stimulation recorded from a WT (*A*), a *mdx-1* (*B*), a *mdx-2* (*D*), an *utr*$^{-/-}$*/mdx-1* (*C*), and an *utr*$^{-/-}$*/mdx-2* (*E*) fiber. AP peak, AP FDHM, ΔF/F peak, ΔF/F FDHM values for each of these experiments were 128 mV, 2.46 ms, 0.75, 1.83 ms (WT); 119 mV, 2.07 ms, 0.59, 1.44 ms (*mdx-1*); 120 mV, 3.33 ms, 0.52, 2.1 ms (*mdx-2*); 120 mV, 1.95 ms, 0.52, 1.5 ms (*utr*$^{-/-}$*/mdx-1*); 112 mV, 4.26 ms, 0.60, 2.07 ms (*utr*$^{-/-}$*/mdx-2*).

mV) are recorded from control fibers. Furthermore, membrane potential values at the interpulse repolarizations are maintained at a slightly depolarized level of approximately −70 mV throughout the train (Fig. 5*A*). For the same fiber, OGB-5N transients elicited by the train of APs are shown in Fig. 5*D*; unlike the APs, the peak values of the OGB-5N transients decay significantly along the train and the ΔF/F values between consecutive transients (interpulse ΔF/F) along the train increases, altogether making the amplitude of the OGB-5N transients (solid circles, Fig. 5*D*) to decay drastically during the train. Interestingly, the largest drop in amplitude of the OGB-5N transients is seen between the first and second pulse of the train, yielding an estimated A_2/A_1 ratio of ~0.5.

When the same pattern of stimulation was applied to fibers from *utr*$^{-/-}$*/mdx* mice, two paradigms of electrical and optical responses were recorded. The APs of *utr*$^{-/-}$*/mdx*-1 fibers (Fig. 5*B*) followed a pattern comparable to that observed in WT fibers. The only appreciable difference is that the interpulse membrane potential (approximately −65 mV) is slightly more positive than that typically observed in WT fibers. Furthermore, other than the fact that OGB-5N transients are significantly smaller than those recorded from WT fibers (as described previously for single AP stimulation), in *utr*$^{-/-}$*/mdx*-1 fibers the A_2/A_1 ratio (~0.5) and the subsequent decay of the amplitude of the Ca^{2+} transients are similar to those seen in WT fibers as can be appreciated by comparing the solid circles in Fig. 5, *D* and *E*. In contrast, *utr*$^{-/-}$*/mdx-2* fibers (Fig. 5, *C* and *F*) demonstrate smaller AP amplitudes and more depolarized interpulse membrane potentials (approximately −55 mV) along the train, in a pattern that is unlike that observed in WT and *utr*$^{-/-}$*/mdx*-1 fibers. In addition, Ca^{2+} transients from *utr*$^{-/-}$*/mdx-2* fibers display a significantly smaller A_2/A_1 ratio (~0.3), which is contrasted by a relatively smaller decay in the amplitude of the transients thereafter, until it reaches a value of ~17% that of the first transient at the end of the train (solid circles in Fig. 5*F*).

Figure 6 display the time dependence of average data, measured in response to 100-Hz stimulation, from WT (n = 11), *mdx-1* (n = 9), *mdx-2* (n = 3), *utr*$^{-/-}$*/mdx-1* (n = 5), and *utr*$^{-/-}$*/mdx-2* (n = 6) fibers. It can be observed that the properties of the APs and Ca^{2+} transients during the train were highly conserved among WT fibers (Fig. 6, *A* and *D*). For them, the A_2/A_1 value was 0.45 ± 0.05; thereafter, the amplitude of the OGB-5N transients decays until it reaches steady values of ~15% that of the first transient at the end of the train (Fig. 6*D*). This secondary decay process was fitted to a single exponential function with a decay time constant (τ) of 176 ± 79 ms (n = 11). Conversely, pooled data from single and double mutant mice (*mdx* and *utr*$^{-/-}$*/mdx*) illustrate that the two different patterns of electrical and optical responses described in Fig. 5 for individual *utr*$^{-/-}$*/mdx* fibers are preserved in the overall fiber populations. Namely, electrical responses from *group 1* fibers from both *mdx* and *utr*$^{-/-}$*/mdx* (solid symbols, Fig. 6, *B* and *C*) are similar between them and with those recorded in WT fibers (Fig. 6*A*). OGB-5N transients of *group 1* fibers display values of A_2/A_1 (0.42 ± 0.05 for *mdx-1*, 0.43 ± 0.08

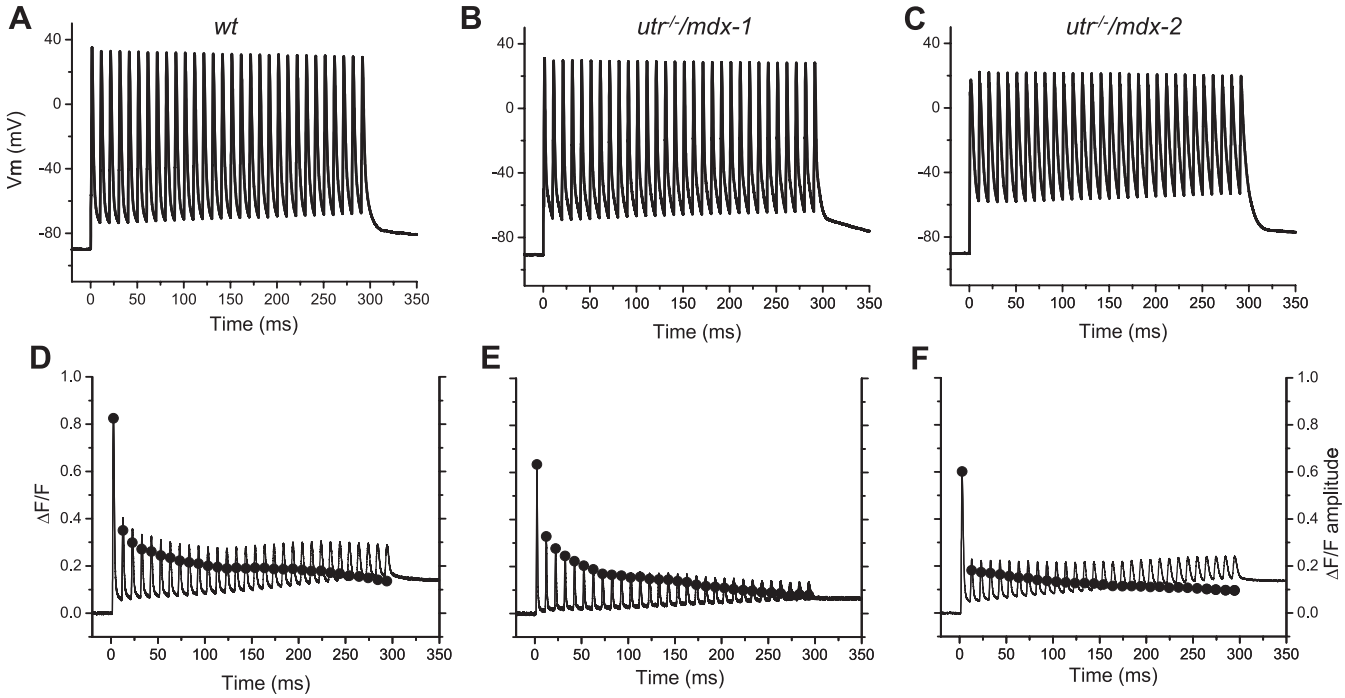

Fig. 5. APs and OGB-5N transients elicited by a train of high-frequency pulses. APs (solid traces, *A–C*) and corresponding OGB-5N (solid traces in *D–F*) elicited by trains of 30 pulses applied at 100 Hz. Data from WT, *utr*$^{-/-}$*/mdx-1,* and *utr*$^{-/-}$*/mdx-2* fibers are shown in *A* and *D*, *B* and *E*, and *C* and *F*, respectively. Filled circles in *D–F* represent the amplitude of OGB-5N transients.

for *utr*$^{-/-}$*/mdx-1*), and decay time constant (τ = 119 ± 41 ms for *mdx-1*, τ = 174 ± 83 ms for *utr*$^{-/-}$*/mdx-1*), which are comparable to those in WT fibers. In contrast, the features of the APs elicited in *group 2* fibers by 100-Hz stimulation (empty symbols, Fig. 6, *B* and *C*) are significantly different to those of APs from WT fibers. It can be seen that *mdx-2* fibers show the larger differences in peak AP, whereas *utr*$^{-/-}$*/mdx-2* fibers show the more depolarized interpulse potential (compare

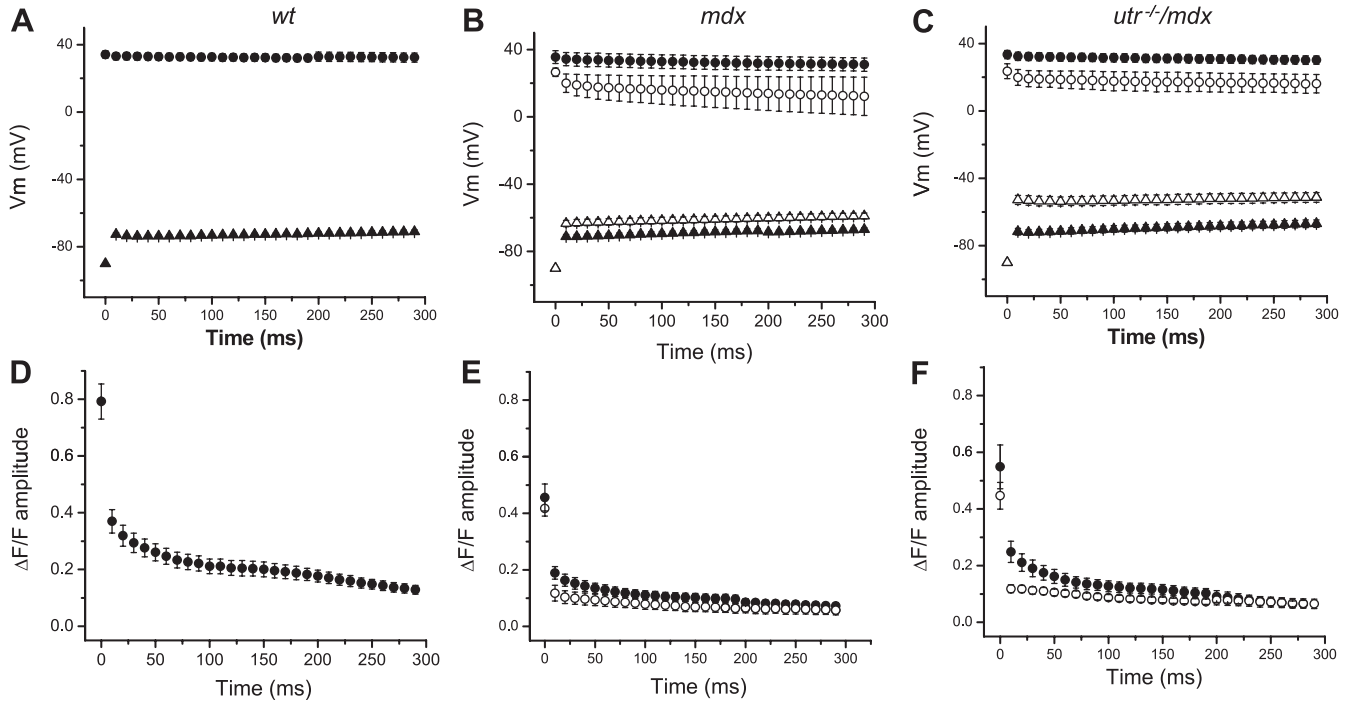

Fig. 6. Peak and interpulse values of APs and OGB-5N transients during high-frequency stimulation. *A–C*: pooled data of the mean peak values (circles) and interpulse potentials (triangles) of APs recorded in response to 100-Hz stimulation from WT (n = 8); *mdx-1* (closed symbols, n = 8), and *mdx-2* (open symbols, n = 3); and *utr*$^{-/-}$*/mdx-1* (closed symbols, n = 3) and *utr*$^{-/-}$*/mdx-2* (open symbols, n = 3). *D–F* corresponding mean amplitude values of pooled data (circles) of OGB-5N transient recorded in correspondence to data in *A–C* respectively. Symbols represent means ± SE.

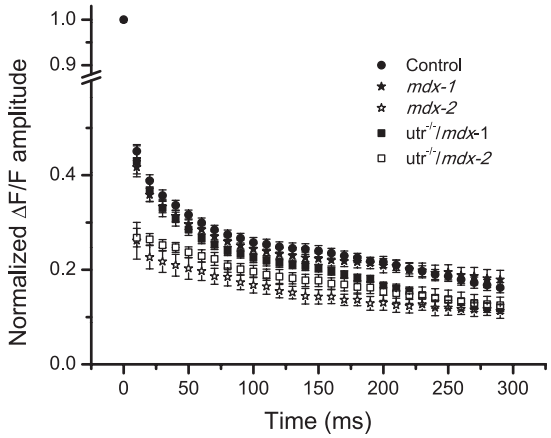

Fig. 7. Normalized amplitudes of OGB-5N transients in WT, *mdx,* and *utr*$^{-/-}$*/mdx* during high-frequency trains. Superimposed pooled data of the normalized amplitudes of OGB-5N transients recorded in response to 100-Hz stimulation from WT (filled circles), *mdx-1* (filled stars), *mdx-2* (open stars), *utr*$^{-/-}$*/mdx-1* (filled squares), and *utr*$^{-/-}$*/mdx-2* (open squares) fibers.

AP peaks and interpulse potentials in Fig. 6, *B* and *C*). Also, OGB-5N transients from *mdx-2* and *utr*$^{-/-}$*/mdx-2* fibers display smaller A_2/A_1 values (0.26 ± 0.07 and 0.27 ± 0.05, respectively) and shorter time constants at the subsequent decay (103 ± 69 ms, 103 ± 53 ms, respectively), with respect to *group 1* and WT fibers (Fig. 6, *D–F*). To facilitate a more in-depth comparison of the process of decay in the amplitude of OGB-5N transients during the train of APs in fibers from WT, *mdx*, and *utr*$^{-/-}$*/mdx* mice, the data from Fig. 6, *D–F*, were normalized and superimposed in Fig. 7. It can be observed that during the first ~50 ms of the tetanic stimulation, the decay in both *mdx-1* and *utr*$^{-/-}$*/mdx-1* fibers is comparable to that observed in WT fibers but significantly different from those in *mdx-2* and *utr*$^{-/-}$*/mdx-2* fibers. Interestingly, after ~100 ms, whereas the amplitudes of the transients in *mdx-1* fibers decay similarly to WT fibers, those in *utr*$^{-/-}$*/mdx-1* fibers decay abruptly to reach values comparable to those of both *mdx-2* and *utr*$^{-/-}$*/mdx-2* fibers.

Rate of Ca^{2+} release during high-frequency trains. To assess the impact that the lack of both dystrophin and utrophin had on the Ca^{2+} release mechanisms of adult mammalian muscle fibers, we compared the Ca^{2+} release fluxes underlying OGB-5N transients recorded from WT and *utr*$^{-/-}$*/mdx* fibers. Representative results, shown in Fig. 8, *A*–C, were calculated from the data in Fig. 5, *D–F*, respectively. For a typical WT fiber (Fig. 8*A*), the peak Ca^{2+} release for the first transient of the train was ~230 μM/ms. This value falls to ~109 μM/ms at the second transient, and decays progressively thereafter reaching ~35 μM/ms at the end of the train (Fig. 8*A*). As shown in Table 3, the Ca^{2+} release flux calculated in response to a single stimulus, or the first stimulus of a train, is always significantly smaller for fibers from mutant mice than for WT fibers. A value of ~175 μM/ms was calculated for the *utr*$^{-/-}$*/mdx-1* and *utr*$^{-/-}$*/mdx-2* fibers shown in Fig. 8, *B* and *C*, which is ~24% smaller than those from WT mice. It should be noted that *group 1* displayed a drop in peak Ca^{2+} release to approximately ~100 μM/ms in the second transient and ~31 μM/ms at the end of the train. In contrast, *group 2* fibers displayed an abrupt depression in the Ca^{2+} release to ~49 μM/ms at the second transient and reached ~19 μM/ms at the end of the train.

APs and Ca^{2+} transients in fibers stimulated at 50 Hz. It could be reasoned that the electrical responses and OGB-5N transients recorded from *group 2* fibers (from both *mdx* and *utr*$^{-/-}$*/mdx* mice) in response to trains of repetitive stimulation would be less impacted by the prolongation of individual APs if the frequency of stimulation is reduced. To verify if this is the case, fibers from the three mice strains were stimulated with trains of 30 pulses at 50 Hz. Interestingly, unlike what was shown for 100 Hz (Fig. 6), at 50 Hz, the peak and interpulse values of APs (Fig. 9, *B–C*) and the amplitudes of OGB-5N transients (Fig. 9, *E–F*) recorded from *groups 1* and *2* fibers became more similar to each other. In fact, for *mdx* mice, the differences in the features of APs and OGB-5N transients recorded from the *mdx-1* and *mdx-2* fibers become negligible. For *utr*$^{-/-}$*/mdx* mice, the difference in the amplitude of the OGB-5N transients (Fig. 9*F*) between *groups 1* and *2* fibers is smaller than that seen at 100 Hz but still significant for the first 60 ms of the train ($P < 0.05$). In addition, the A_1/A_2 ratios of OGN-5N transients recorded from fibers belonging to the five fibers' populations [0.57 ± 0.04 (n = 11), 0.56 ± 0.04 (n = 9), 0.50 ± 0.04 (n = 3), 0.61 ± 0.04 (n = 5), and 0.50 ± 0.03 (n = 5) for WT, *mdx-1*, *mdx-2*, *utr*$^{-/-}$*/mdx-1*, *and utr*$^{-/-}$*/mdx-2* fibers, respectively] are quite similar when using 50 Hz stimulation.

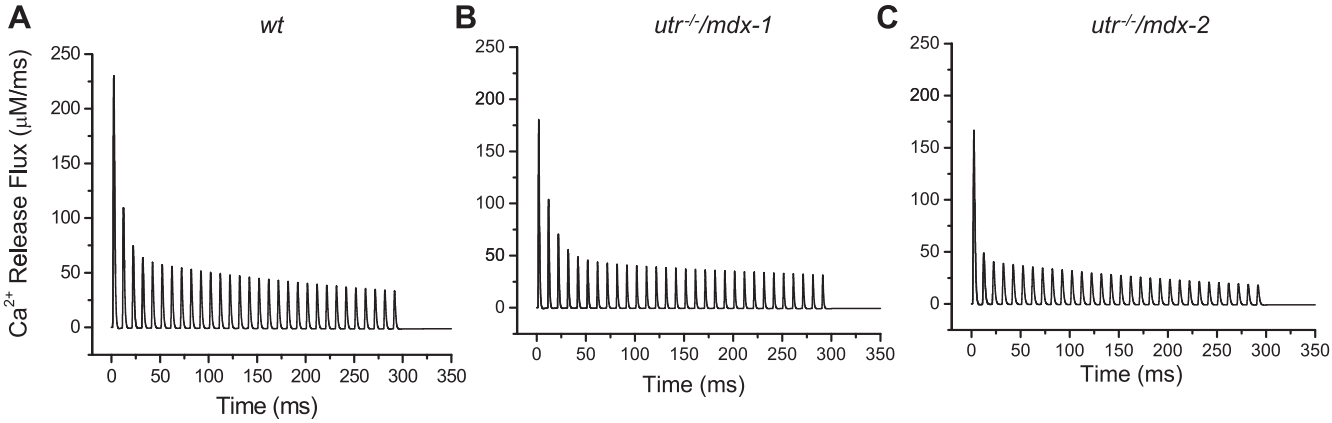

Fig. 8. Ca^{2+} release fluxes and total [Ca] changes calculated from transients at 100 Hz stimulation. *A–C*: Ca^{2+} release fluxes used to simulate the OGB-5N transients from WT, *utr*$^{-/-}$*/mdx-1*, and *utr*$^{-/-}$*/mdx*-2 fibers as shown in Fig. 5, *D–F*, respectively.

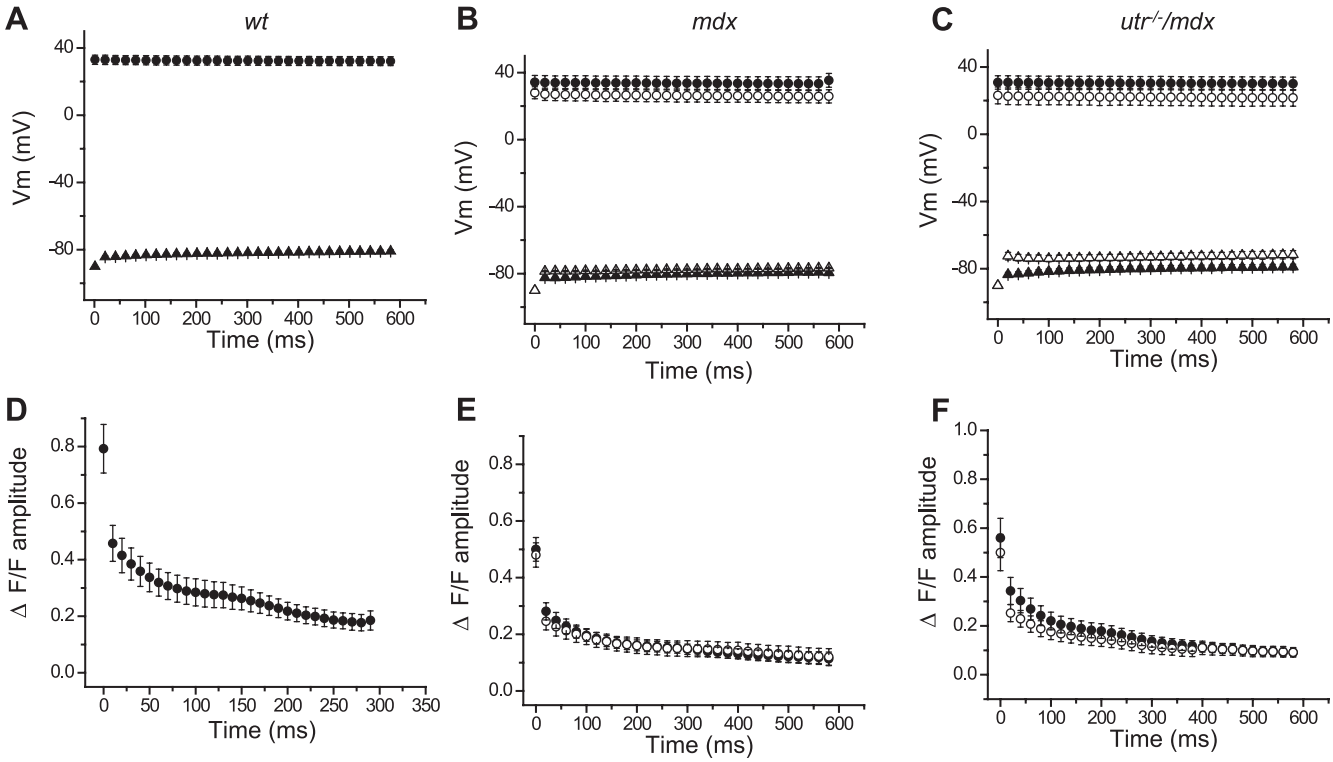

Fig. 9. Peak and interpulse values of APs and OGB-5N transients during 50 Hz stimulation. *A–C*: pooled data of the mean peak values (circles) and interpulse potentials (triangles) of APs recorded in response to 50-Hz stimulation from WT (closed symbols, $n = 6$); *mdx-1* (closed symbols, $n = 8$) and *mdx-2* (open symbols, $n = 3$); and $utr^{-/-}$*/mdx-1* (closed symbols, $n = 5$) and $utr^{-/-}$*/mdx-2* (open symbols, $n = 3$). *D–F* shows the corresponding mean amplitude values of pooled data of OGB-5N transient recorded in correspondence to data in *A–C* respectively. Symbols represent means ± SE.

DISCUSSION

Until now, studies comparing the mechanisms of excitability and EC coupling in fibers from $utr^{-/-}$*/mdx* mice, with respect to those of WT and *mdx* animals, have been lacking. The present work was aimed to fill this void by comparatively studying the three mice strains. We found that FDB muscles from either *mdx* or $utr^{-/-}$*/mdx* mice display heterogeneous populations of fibers, which could be divided in two groups based on the properties of the electrical responses to single pulses and repetitive stimulation. The APs amplitude and FDHM in *group 1* fibers were found to be similar to those from WT fibers (Fig. 4, Table 3). *Group 2* fibers, on the other hand, display smaller and longer-lasting APs than those recorded in WT and *group 1* fibers (Fig. 4, Table 3). Nonetheless, these differences were more noticeable in fibers from $utr^{-/-}$*/mdx* mice (Fig. 4, Table 3).

The exact mechanisms underlying the reduction in amplitude and the prolongation of the APs recorded from *group* 2 fibers are unknown, but they could stem from alterations in the expression, targeting, and/or functional properties of the $Na_V1.4$ channel eventually related to variability in the expression of syntrophins and/or other regulatory proteins in dystrophic fibers (15, 21, 24). In this regard, the proposal by Riboux et al. (24) that an unbalance in the expression of syntrophins may lead to functional deficits in $Na_V1.4$ channels in *mdx* fibers could provide an explanation for the limitations seen in the *mdx-2* fibers. Unfortunately, there are no reports about the expression of syntrophins in $utr^{-/-}$*/mdx* mice, but it seems feasible that a more profound disarrangement of these proteins associated with the absence of both dystrophin and utrophin may lead to more severe dysregulation of $Na_V1.4$, thus explaining the smaller and longer APs recorded from $utr^{-/-}$*/mdx-2* fibers. The question that remains though, is why the electrical responses from *group 1* fibers from both *mdx* and $utr^{-/-}$*/mdx* mice are spared from these deficits? New experiments using voltage-clamp conditions and potentiometric dyes to evaluate the $Na_V1.4$ channel properties (amplitude, kinetics, and voltage dependence of the sodium currents) and estimate the channel density at the surface and TTS membranes (26), in parallel with the use of immunohystochemical analysis to test for syntrophins' expression and location, will be necessary to unveil these important mechanistic issues.

In contrast to what we found regarding APs, we observed that the reduction in Ca^{2+} release elicited by single pulse stimulations is similar for both *mdx* and $utr^{-/-}$*/mdx* mice, regardless of the fiber group (*group 1* or *2*; see Table 3). Although the exact mechanisms leading to the Ca^{2+} release impairment observed in both mouse strains remain to be determined, our laboratory has already demonstrated in *mdx* fibers that alterations in the AP conduction in the TTS, in the voltage dependence of the transduction process at the triads, and in the SR Ca^{2+} content, do not seem to be critical causes (9, 27, 29, 30). Consequently, we speculate that in fibers from *mdx* mice, the Ca^{2+} release limitation is probably confined to the altered expression or physiological dysregulation of the RyR1 Ca^{2+} release channel (29). From the similarity of results presented here for *mdx* and $utr^{-/-}$*/mdx* fibers, it seems possible to suggest that the Ca^{2+} release impairments may have a

common root for both strains of mice. However, more extensive experiments, similar to those already done in *mdx* fibers (9, 27, 29, 30), will be necessary to ultimately verify this hypothesis.

Total [Ca^{2+}] changes calculated from single pulse transients in WT, *mdx,* and *utr*$^{-/-}$*/mdx* fibers were (in μM): 341 ± 79 (n = 15), 238 ± 40 (n = 11), and 261 ± 71 (n = 14), respectively; thus, mutant fibers release ~70% the total Ca^{2+} per AP compared with normal fibers. These values, and that of the peak Ca^{2+} release flux in WT fibers (242 ± 58 μM/ms) are in close agreement with those calculated by other authors for EDL muscle fibers (346 ± 6 μM and 212 ± 4 μM/ms, respectively; means ± SE, 16°C) using a similar single compartment model (3). This coincidence of results for WT fibers not only reinforces the validity of calculations made from data obtained under different experimental conditions, but it also suggests that the reduction in peak Ca^{2+} fluxes (and total [Ca^{2+}] changes) reported here for *mdx* and *utr*$^{-/-}$*/mdx* fibers are not accounted for by the abnormal upregulation of genes encoding proteins typical of slow muscles (2, 23) since slow-twitch fibers show significantly smaller values for both calculations (70 μM/ms and 127 μM; Ref. 3). Our results are in general agreement with reports suggesting that the specific twitch force in fast muscles (EDL) from *mdx* and *utr*$^{-/-}$*/mdx* mice is comparable but smaller than that in WT muscles (7). An important conclusion from the above observations is that the Ca^{2+} release impairment observed with single pulse stimulation in *mdx* fibers is not significantly ameliorated by the overexpression of utrophin. This unanticipated result is apparently inconsistent with the claimed role that utrophin is an equivalent functional substitute of dystrophin in muscles from *mdx* mice (6, 7, 12, 22). However, as discussed below, the presence of utrophin seems to improve the ability of *mdx-1* fibers to sustain Ca^{2+} release during longer periods of 100-Hz tetanic stimulation.

Regarding *mdx* fibers, the data presented in this paper using 30 mM EGTA are in good agreement with previous results from our laboratory using different ethylene glycol-bis(β-aminoethyl ether)-*N,N,N′,N′*-tetraacetic acids but otherwise similar experimental conditions (30). We found here that *mdx* fibers display 38% depression of both OGB-5N transients and peak Ca^{2+} flux, which are comparable to the 43% and 45% depression for the same respective parameters obtained previously using 5 mM ethylene glycol-bis(β-aminoethyl ether)-*N,N,N′,N′*-tetraacetic acid (30). Nonetheless, our data are at odds with those recently obtained from intact EDL fibers from *mdx* mice (16); these authors report a smaller depression (~26%) of the peak Ca^{2+} flux. Whereas this discrepancy is intriguing, it may stem from differences in the methodology used to record Ca^{2+} signals.

Since discharge frequencies up to 100 Hz have been measured in motoneurons from ambulant rodents (14), we measured the electrical activity and calcium release elicited by this frequency. Experiments using this frequency of stimulation revealed that fibers from WT animals showed a very uniform pattern of electrical and optical responses. In contrast, fibers from *utr*$^{-/-}$*/mdx* mice, and to a lesser extent those from *mdx* mice, exhibited heterogeneous patterns of responses. In general, *group 1* fibers behaved similarly to WT fibers (Fig. 7, solid symbols) with the exception of *utr*$^{-/-}$*/mdx-1* fibers in which the Ca^{2+} transients show an abrupt decay toward values similar to those of *group 2* fibers after ~60 ms. We propose that the limitation in the ability to sustain Ca^{2+} release during a high-frequency tetanus, which is not observed in *mdx-1* fibers, is linked to the lack of expression of utrophin in these fibers; this argues for a role of this protein on the preservation of EC coupling mechanisms during repetitive stimulation as they may occur in vivo.

Group 2 fibers, on the other hand, displayed Ca^{2+} responses with highly reduced A_2/A_1 ratio and depressed amplitudes during the first 50 ms of the train. It seems reasonable to hypothesize that the abrupt limitation in amplitude of the Ca^{2+} transients during the 100-Hz trains observed in *group 2* fibers may be linked to the reduced amplitude and increased duration of the APs (already suggested to emerge from the absence of dystrophin and/or utrophin in these fibers). In support of these ideas, differences in the pattern of Ca^{2+} release during trains of 30 pulses between *group 1* and *group 2* mutant fibers became almost unnoticeable at 50 Hz (Fig. 9) or lower frequencies of stimulation (data not shown). Though the actual cause(s) for the prolongation of the APs in *group 2* fibers is (are) unknown yet, our results suggests that this alteration may lead to an increased limitation of Ca^{2+} release at high frequencies of stimulation. Interestingly, our data showing that the proportion of *group 2* fibers is significantly larger in *utr*$^{-/-}$*/mdx* than in *mdx* muscles (Table 3), coupled with these fibers' severe limitations at high-frequency stimulations (Figs. 6 and 8), are in good agreement with data showing that the depression of tetanic tension is more marked for *utr*$^{-/-}$*/mdx* than *mdx* muscles during 300 ms, 125-Hz trains (7).

In summary, fibers from *utr*$^{-/-}$*/mdx* mice seem to display more pervasive alterations in the EC coupling than those observed in the *mdx* model; these limitations would have been unnoticed by not using high-frequency stimulation but are quite relevant to the functional performance of the muscle fibers under CNS control.

ACKNOWLEDGMENTS

The authors are indebted with Dr. J. R. Sanes (Washington University, St. Louis, MO) and Dr. M. Spencer (UCLA) for sharing DKO specimens that allowed us to establish a colony in our laboratory. We also thank Marbella Quinonez for helpful discussions.

GRANTS

This work was supported by National Institutes of Health grants AR-047664 and AR-054816 (NIAMS) and GM-074706 (NIGMS).

DISCLOSURES

No conflicts of interest are declared by the author(s).

REFERENCES

1. **Amalfitano A, Chamberlain JS.** The mdx-amplification-resistant mutation system assay, a simple and rapid polymerase chain reaction-based detection of the mdx allele. *Muscle Nerve* 19: 1549–1553, 1996.
2. **Baker PE, Kearney JA, Gong B, Merriam AP, Kuhn DE, Porter JD, and Rafael-Fortney JA.** Analysis of gene expression differences between utrophin/dystrophin-deficient vs. mdx skeletal muscles reveals a specific upregulation of slow muscle genes in limb muscles. *Neurogenetics* 7: 81–91, 2006.
3. **Baylor SM, Hollingworth S.** Sarcoplasmic reticulum calcium release compared in slow-twitch and fast-twitch fibres of mouse muscle. *J Physiol* 551: 125–138, 2003.
4. **Capote JC, DiFranco M, Vergara JL.** The absence of utrophin does not further the impairment of Ca^{2+} release displayed by mdx muscle. *Biophys J* 96: 236a–236a, 2009.

5. **Collins CA, Morgan JE.** Duchenne's muscular dystrophy: animal models used to investigate pathogenesis and develop therapeutic strategies. *Int J Exp Pathol* 84: 165–172, 2003.
6. **Deconinck AE, Rafael JA, Skinner JA, Brown SC, Potter AC, Metzinger L, Watt DJ, Dickson JG, Tinsley JM, Davies KE.** Utrophin-dystrophin-deficient mice as a model for Duchenne muscular dystrophy. *Cell* 90: 717–727, 1997.
7. **Deconinck N, Rafael JA, Beckers-Bleukx G, Kahn D, Deconinck AE, Davies KE, Gillis JM.** Consequences of the combined deficiency in dystrophin and utrophin on the mechanical properties and myosin composition of some limb and respiratory muscles of the mouse. *Neuromuscul Disord* 8: 362–370, 1998.
8. **DiFranco M, Capote J, Vergara JL.** Optical imaging and functional characterization of the transverse tubular system of mammalian muscle fibers using the potentiometric indicator di-8-ANEPPS. *J Membr Biol* 208: 141–153, 2005.
9. **DiFranco M, Woods CE, Capote J, Vergara JL.** Dystrophic skeletal muscle fibers display alterations at the level of calcium microdomains. *Proc Natl Acad Sci USA* 105: 14698–14703, 2008.
10. **Emery AE.** The muscular dystrophies. *Lancet* 359: 687–695, 2002.
11. **Escobar AL, Velez P, Kim AM, Cifuentes F, Fill M, Vergara JL.** Kinetic properties of DM-nitrophen and calcium indicators: rapid transient response to flash photolysis. *Pflügers Arch* 434: 615–631, 1997.
12. **Grady RM, Merlie JP, Sanes JR.** Subtle neuromuscular defects in utrophin-deficient mice. *J Cell Biol* 136: 871–882, 1997.
13. **Grady RM, Teng H, Nichol MC, Cunningham JC, Wilkinson RS, Sanes JR.** Skeletal and cardiac myopathies in mice lacking utrophin and dystrophin: a model for Duchenne muscular dystrophy. *Cell* 90: 729–738, 1997.
14. **Hennig R, Lomo T.** Firing patterns of motor units in normal rats. *Nature* 314: 164–166, 1985.
15. **Hirn C, Shapovalov G, Petermann O, Roulet E, Ruegg Nav1 UT. 4.** Deregulation in dystrophic skeletal muscle leads to Na+ overload and enhanced cell death. *J Gen Physiol* 132: 199–208, 2008.
16. **Hollingworth S, Zeiger U, Baylor SM.** Comparison of the myoplasmic calcium transient elicited by an action potential in intact fibres of mdx and normal mice. *J Physiol* 586: 5063–5075, 2008.
17. **Keep NH.** Structural comparison of actin binding in utrophin and dystrophin. *Neurol Sci* 21: S929–S937, 2000.
18. **Khurana TS, Davies KE.** Pharmacological strategies for muscular dystrophy. *Nat Rev Drug Discov* 2: 379–390, 2003.
19. **Nagerl UV, Novo D, Mody I, Vergara JL.** Binding kinetics of calbindin-D(28k) determined by flash photolysis of caged Ca(2+). *Biophys J* 79: 3009–3018, 2000.
20. **O'Brien KF, Kunkel LM.** Dystrophin and muscular dystrophy: past, present, and future. *Mol Genet Metab* 74: 75–88, 2001.
21. **Peters MF, Adams ME, Froehner SC.** Differential association of syntrophin pairs with the dystrophin complex. *J Cell Biol* 138: 81–93, 1997.
22. **Rafael JA, Tinsley JM, Potter AC, Deconinck AE, Davies KE.** Skeletal muscle-specific expression of a utrophin transgene rescues utrophin-dystrophin deficient mice. *Nat Genet* 19: 79–82, 1998.
23. **Rafael JA, Townsend ER, Squire SE, Potter AC, Chamberlain JS, Davies KE.** Dystrophin and utrophin influence fiber type composition and post-synaptic membrane structure. *Hum Mol Genet* 9: 1357–1367, 2000.
24. **Ribaux P, Bleicher F, Couble ML, Amsellem J, Cohen SA, Berthier C, Blaineau S.** Voltage-gated sodium channel (SkM1) content in dystrophin-deficient muscle. *Pflügers Arch* 441: 746–755, 2001.
25. **van Deutekom JC, van Ommen GJ.** Advances in Duchenne muscular dystrophy gene therapy. *Nat Rev Genet* 4: 774–783, 2003.
26. **Vergara JL, Capote J, DiFranco M.** Characterization of the Na and K delayed rectifier conductances of mammalian skeletal muscle fibers' transverse tubular system using the potentiometric indicator di-8-ANEPPS. *Biophys J* 92: 22a, 2007.
27. **Vergara JL, DiFranco M.** Sarcoplasmic reticulum calcium content in normal and dystrophic mammalian skeletal muscle fibers. *Biophys J* 96: 235a–236a, 2009.
28. **Watchko JF, O'Day TL, Hoffman EP.** Functional characteristics of dystrophic skeletal muscle: insights from animal models. *J Appl Physiol* 93: 407–417, 2002.
29. **Woods CE, Novo D, DiFranco M, Capote J, Vergara JL.** Propagation in the transverse tubular system and voltage dependence of calcium release in normal and mdx mouse muscle fibres. *J Physiol* 568: 867–880, 2005.
30. **Woods CE, Novo D, DiFranco M, Vergara JL.** The action potential-evoked sarcoplasmic reticulum calcium release is impaired in mdx mouse muscle fibres. *J Physiol* 557: 59–75, 2004.